Dinuclear Oxomolybdenum(V) Complexes Showing Strong Interactions across Diphenol Bridging Ligands: Syntheses, Structures, Electrochemical Properties, and EPR Spectroscopic Properties

Văn Ân Ung, David A. Bardwell, John C. Jeffery, John P. Maher, Jon A. McCleverty,* Michael D. Ward,* and Andrew Williamson

School of Chemistry, University of Bristol, Cantock's Close, Bristol BS8 1TS, U.K.

Received December 21, 1995[⊗]

We have prepared a series of dinuclear complexes [{Mo^{V}(O)(Tp*)Cl}(μ-**OO**)], where "**OO**" represents one of the series of diphenolate bridging ligands [1,4-O(C_6H_4)$_n$O]$^{2-}$ (n = 1−4; complexes **1**−**4**, respectively), [O(C_6H_3-2-Me)$_2$O]$^{2-}$ (complex **5**), or [1,3-OC_6H_4O]$^{2-}$ (complex **6**) [Tp* = tris(3,5-dimethylpyrazolyl)hydroborate]. The complexes therefore contain two paramagnetic (d^1), redox-active metal centers. For complexes **1**−**4** the metal−metal separation increases due to the increasing number of phenyl spacers in the bridge. Complex **5** is similar to **2** with the exception that for steric reasons there is a larger dihedral twist between the halves of the complex. Complex **6** is similar to **1**, but with a *meta* substitution pattern at the bridging ligand instead of *para*. Complexes **1** and **6** were characterized by X-ray crystallography. For **1**·2Et_2O: $C_{44}H_{68}B_2Cl_2Mo_2N_{12}O_6$; orthorhombic, *Pnnm*; a = 24.566(11), b = 8.085(4), c = 14.172(4) Å; Z = 2. For **6**·3CH_2Cl_2: $C_{39}H_{54}B_2Cl_8Mo_2N_{12}O_4$; monoclinic, $P2_1/n$; a = 15.984(3), b = 16.934(3), c = 20.931(3) Å, β = 105.33(1)°; Z = 4. Due to the cocrystallization of the two diastereoisomers of the complexes (the Mo centers are chiral), disorder is present in both cases between the oxo and chloride ligands which could be completely resolved for **6** but not for **1**. Electrochemical measurements showed that each Mo(V) center undergoes a one-electron oxidation [to Mo(VI)] and a one-electron reduction [to Mo(IV)]. Electrochemical interactions across the bridge result in very large splittings between the two oxidations (e.g. 990 mV for **1**) and smaller but still significant splittings between the reductions (e.g. 250 mV for **1**). The much stronger interaction between the oxidation processes is due to the fact that they are partly delocalized onto the bridging ligand, whereas the reduction processes are almost completely metal-localized. EPR spectra of the complexes showed the presence of magnetic exchange between the paramagnetic centers, with several features characteristic of magnetic exchange: the hyperfine pattern, line broadening, and the presence of a half-field (Δm_s = 2) transition. The magnitudes of the electrochemical interactions and of the magnetic interactions could be related to the structures (length, substitution pattern, dihedral twist) of the bridging ligands.

Introduction

A major goal of coordination chemistry is to prepare multinuclear complexes in which the interactions between component parts lead to novel or useful properties. Electrochemical,[1] photochemical,[2] and magnetic[3] interactions between remote metal centers all ultimately depend on either transfer of one electron or interaction between two or more electrons, between the interacting centers. Usually this interaction is mediated by a bridging ligand, so it is of fundamental importance to understand the role of the bridging ligand and how it can modify or control the interactions across it.

In recent papers we described the electrochemical, spectroscopic, and magnetic properties of polynuclear complexes in which two or more paramagnetic {Mo(NO)(Tp*)Cl} fragments are coordinated to the binding sites (pyridyl, phenolate, amide) of various multinucleating bridging ligands.[4] Such complexes show exceptionally strong electrochemical and magnetic interactions between the molybdenum end groups: for example, in [{Mo(NO)(Tp*)Cl}$_2$(μ-4,4′-bipy)] (bipy = bipyridine) the two (formally metal-centered) one-electron reductions are separated by 765 mV,[4e] and there is an antiferromagnetic exchange interaction with $J = -33$ cm^{-1}.[4f] The unusually high magnitude of the interactions between the {Mo(NO)(Tp*)Cl} end groups has allowed us to prepare complexes with a variety of bridging ligands and to relate the magnitudes of the electrochemical and magnetic interactions between the remote metal centers to features of the bridging ligands such as length, degree of conjugation, dihedral twists between aromatic rings, substitution pattern, and symmetry.[4]

However for computational purposes, such as molecular orbital calculations, the {Mo(NO)(Tp*)Cl} fragment presents problems because of the noninnocence of the nitrosyl ligand

[⊗] Abstract published in *Advance ACS Abstracts,* August 1, 1996.

(1) (a) Ward, M. D. *Chem. Soc. Rev.* **1995**, *34*, 121. (b) Kalyanasundaram, K.; Nazeeruddin, M. K. *Inorg. Chim. Acta* **1994**, *226*, 213.

(2) (a) Sauvage, J.-P.; Collin, J.-P.; Chambron, J.-C.; Guillerez, S.; Coudret, C.; Balzani, V.; Barigelletti, F.; De Cola, L.; Flamigni, L. *Chem. Rev.* **1994**, *94*, 993. (b) Balzani, V.; Scandola, F. *Supramolecular Photochemistry*; Ellis Horwood: Chichester, U.K., 1991.

(3) (a) Kahn, O. *Molecular Magnetism*; VCH Publishers, Inc.: New York, 1993. (b) McCusker, J. K.; Schmitt, E. A.; Hendrickson, D. N. In *Magnetic Molecular Materials*; Gatteschi, D., Kahn, O., Miller, J. S., Palacio, F., Eds.; NATO ASI Series E198; Kluwer Academic Press: Dordrecht, The Netherlands, 1991; p 297. (c) Kahn, O.; Pei, Y.; Journaux, Y. In *Inorganic Materials;* Bruce, D. W, O'Hare, D., Eds.; Wiley: Chichester, U.K., 1992; p 59. (d) Bushby, R. J.; Paillaud, J.-L. In *Introduction to Molecular Electronics;* Petty, M. C., Bryce, M. R., Bloor, D., Eds.; Edward Arnold: London, 1995; p 72.

(4) (a) Amoroso, A. J.; Cargill Thompson, A. M. W.; Maher, J. P.; McCleverty, J. A.; Ward, M. D. *Inorg. Chem.* **1995**, *34*, 4828. (b) Bhadbhade, M. M.; Das, A.; Jeffery, J. C.; McCleverty, J. A.; Navas Badiola, J. A.; Ward, M. D. *J. Chem. Soc., Dalton Trans.* **1995**, 2769. (c) Cook, R.; Maher, J. P.; McCleverty, J. A.; Ward, M. D.; Wlodarczyk, A. *Polyhedron* **1993**, *12*, 2111. (d) Das, A.; Jeffery, J. C.; Maher, J. P.; McCleverty, J. A.; Schatz, E.; Ward, M. D.; Wollermann, G. *Inorg. Chem.* **1993**, *32*, 2145. (e) Das, A.; Maher, J. P.; McCleverty, J. A.; Navas Badiola, J. A.; Ward, M. D. *J. Chem. Soc., Dalton Trans.* **1993**, 681. (f) Cargill Thompson, A. M. W.; Gatteschi, D.; McCleverty, J. A.; Navas, J. A.; Rentschler, E.; Ward, M. D. *Inorg. Chem.* **1996**, *35*, 2701.

S0020-1669(95)01634-X CCC: $12.00

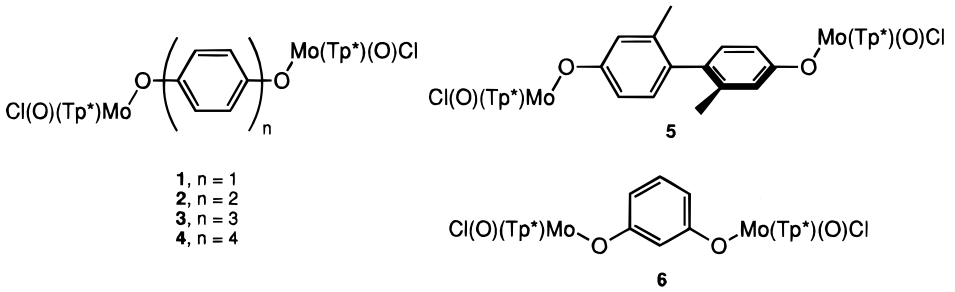

Figure 1. Structural formulas of the complexes described in this paper.

and the resulting difficulty in specifying exactly the oxidation state and electron configuration of the metal. For this reason we have now started to use the $\{Mo^{V}(O)(Tp^*)Cl\}^{+}$ fragment. This was first investigated by Enemark, who prepared a series of mononuclear complexes [Mo(O)(Tp*)ClX] (where X is a monodentate anionic ligand) and determined their electrochemical and spectroscopic properties.[5] This complex fragment was of particular appeal to us because (i) it is electronically simple (d^1), (ii) it is both redox-active and paramagnetic, and so—like the {Mo(NO)(Tp*)Cl} fragment—will lend itself to the study of electrochemical and magnetic interactions across bridging ligands, (iii) it is synthetically easy to use, and (iv) the coordination chemistry and bioinorganic chemistry of oxomolybdenum(V) complexes in general have been extensivly studied, so their spectroscopic properties are fairly thoroughly understood.[6]

Accordingly we have prepared a series of complexes of the type $[\{Mo^{V}(O)(Tp^*)Cl\}_2(\mu\text{-}\mathbf{OO}\}]$, where "**OO**" denotes a bridging ligand with two anionic phenolate-type donors; these range from ligands with one aromatic ring, such as 1,3- and 1,4-dihydroxybenzene, to 4,4‴-dihydroxyquaterphenyl with four *para*-linked aromatic rings in the bridge. The structural formulas of the complexes are summarized in Figure 1. In this paper we describe their synthesis and characterization, the crystal structures of two of the complexes, and their electrochemical and EPR spectroscopic properties and how these vary as a function of the bridging ligand.

Experimental Section

General Details. Instrumentation used for spectroscopic (NMR, UV/vis, EPR, FAB-MS, IR) and electrochemical studies was described earlier.[4a] EPR spectra (X-band) were recorded at microwave frequencies of *ca.* 9.7 GHz (solution spectra) and 9.4 GHz (frozen-glass spectra), such that the field centers for the signals occurred in the region of 3600 G (solution spectra) and 3500 G (frozen-glass spectra). Sample concentrations were typically 10^{-3} mol dm^{-3}; spectra were recorded with a microwave power of 20 mW and a modulation amplitude of 2 G. Multiple scans were recorded and averaged to improve the signal-to-noise ratio: for solution spectra, 25 scans were generally sufficient; for examining very weak $\Delta m_s = 2$ signals, several hundred scans were necessary.

All organic starting materials were obtained from the usual commercial sources (Aldrich, Lancaster, Avocado) and used as received. $[Mo(O)(Tp^*)Cl_2]$[5] and $Ni(dppe)Cl_2$[7] were prepared according to the literature methods.

Ligand Syntheses. (a) 2,2′-Dimethyl-4,4′-dimethoxy-1,1′-biphenyl. This was prepared by homocoupling of 3-methyl-4-bromoanisole with a $Ni(PPh_3)_2Br_2$/Zn catalyst in thf at 50 °C exactly according to a standard procedure used for other aryl halides.[8] After extraction of the reaction mixture with CH_2Cl_2, the crude material was purified by flash chromatography on silica using CH_2Cl_2/hexane (4:1) as eluent (yield: 25%).

(b) 4,4″-Dimethoxy-1,1′:4′,1″-terphenyl. A thf solution of the Grignard reagent 4-$MeOC_6H_4MgBr$ [derived from 4-bromoanisole (4.40 g, 23.5 mmol) and Mg turnings (0.68 g, 28 mmol) in thf (30 cm^3)] was added at 0 °C to a stirred suspension of 1,4-dibromobenzene (2.36 g, 10 mmol) and $Ni(dppe)Cl_2$ (0.32 g, 0.6 mmol) in thf (40 cm^3). The resulting dark brown mixture was stirred overnight at room temperature and was then quenched by addition of ethanol (15 cm^3) and concentrated HCl (1 cm^3). The resulting precipitate was collected by filtration, washed with ethanol, and dried (yield: 60%).

(c) 4,4‴-Dimethoxy-1,1′:4′,1″:4″,1‴-quaterphenyl. A thf solution of the Grignard reagent 4-$MeOC_6H_4MgBr$ [derived from 4-bromoanisole (7.47 g, 40 mmol) and Mg turnings (1.22 g, 50 mmol) in thf (30 cm^3)] was added at 0 °C to a stirred suspension of 4,4′-dibromobiphenyl (3.12 g, 10 mmol) and $Ni(dppe)Cl_2$ (0.32 g, 0.6 mmol) in thf (40 cm^3). The reaction mixture was worked up as above to give a white precipitate, which was washed with ethanol and dried (yield: 50%).

(d) 2,2′-Dimethyl-4,4′-dihydroxybiphenyl, 4,4″-Dihydroxy-1,1′:4′,1″-terphenyl, and 4,4‴-Dihydroxy-1,1′:4′,1″:4″,1‴-quaterphenyl. These were prepared by demethylation of the appropriate dimethoxy compounds (above) with molten pyridinium chloride at 200 °C for 2 h under N_2.[9] In each case, after the mixture was allowed to cool, addition of a large excess of water dissolved the pyridinium chloride and afforded an off-white precipitate of the diphenol ligand, which was collected by filtration, washed with water, and dried. Yields: 70−80%. The products were obtained suffiently pure for use in the complexation reactions, but samples could be recrystallized from MeOH/water if required.

Characterization data for the ligands are summarized in Table 1.

Complex Syntheses. The dinuclear molybdenum complexes were all prepared using a method based on that of Enemark.[5] In each case, a mixture of $[Mo(O)(Tp^*)Cl_2]$, ligand H_2L (0.5 equiv), and dry Et_3N (0.5 cm^3, excess) was heated with stirring under N_2 in dry toluene. The reactions could be followed by tlc (silica, CH_2Cl_2). The minimum temperature necessary was *ca.* 90 °C; in some cases, it was necessary to heat the mixture to reflux to initiate the reaction. After all of the $[Mo(O)(Tp^*)Cl_2]$ was consumed, the mixture was evaporated to dryness and the residue chromatographed on silica with CH_2Cl_2. The dinuclear complexes were the obvious intensely-colored major fractions. Characterisation data, colors, and yields are summarized in Table 2.

Crystallographic Studies. Complexes **1** and **6** afforded crystals suitable for X-ray diffraction by recrystallization from CH_2Cl_2/ether (vapor diffusion). Crystals of **1**·$2Et_2O$ lost solvent very fast, so they were mounted in a sealed capillary tube with a drop of the mother liquor present and were examined at room temperature; crystals of **6**·$3CH_2Cl_2$ were transferred directly from the mother liquor to the diffractometer under a cold stream of N_2 (−100 °C).

Data were collected using a Siemens SMART three-circle diffractometer with a CCD area detector (graphite-monochromatized Mo Kα X-radiation, $\bar{\lambda} = 0.710\ 73$ Å). For **1**·$(Et_2O)_2$ (crystal size 0.25 × 0.25 × 0.05 mm^3) 10 153 data were collected to $2\theta_{max} = 46.5°$ which gave after merging 2119 independent data ($R_{int} = 0.099$); for **6**·$(CH_2Cl_2)_3$

(5) Cleland, W. E., Jr.; Barhhart, K. M.; Yamanouchi, K.; Collison, D.; Mabbs, F. E.; Ortega, R. B.; Enemark, J. H. *Inorg. Chem.* **1987**, *26*, 1017.
(6) (a) Spivack, B.; Dori, Z. *Coord. Chem. Rev.* **1975**, *17*, 99. (b) Steifel, E. I. *Prog. Inorg. Chem.* **1977**, *22*, 1. (c) Pope, M. T. *Prog. Inorg. Chem.* **1991**, *39*, 181.
(7) Van Hecke, G. R.; Horrocks, W. D. *Inorg. Chem.* **1966**, *5*, 1968.
(8) Iyoda, M.; Otsuka, H.; Sato, K.; Nisato, N.; Oda, M. *Bull. Chem. Soc. Jpn.* **1990**, *63*, 80.
(9) Dietrich-Buchecker, C. O.; Sauvage, J.-P. *Tetrahedron* **1990**, *46*, 503.

Table 1. Characterization Data for the New Ligands and Their Methylated Precursors

molecule	^{1}H NMR data, ppm (*J*, Hz) (300 MHz)	*m*/*z* for M^+ (EIMS)
2,2′-dimethyl-4,4′-dimethoxy-1,1′-biphenyl[a]	7.01 (2 H, d, $J = 8.2$; H^6), 6.81 (2 H, d, $J = 2.6$; H^3), 6.76 (2 H, dd, $J = 8.2, 2.6$; H^5), 3.83 (6 H, s; OMe), 2.04 (6 H, s; Me)	242
2,2′-dimethyl-4,4′-dihydroxy-1,1′-biphenyl[b]	9.24 (2 H, s; OH), 6.81 (2 H, d, $J = 8.2$; H^6), 6.67 (2 H, d, $J = 2.4$; H^3), 6.61 (2 H, dd, $J = 8.2, 2.6$; H^5), 1.91 (6 H, s; Me)	214
4,4″-dimethoxy-1,1′:4′,1″-terphenyl[c]	7.62 (4 H, s; $H^{2'/3'/5'/6'}$), 7.59 (4 H, d, $J = 8.6$; $H^{3/5/3''/5''}$), 6.99 (4 H, d, $J = 8.6$; $H^{2/6/2''/6''}$), 3.85 (6 H, s; OMe)	290
4,4″-dihydroxy-1,1′:4′,1″-terphenyl[d]	7.58 (4 H, s; $H^{2'/3'/5'/6'}$), 7.48 (4 H, d, $J = 8.7$; $H^{3/5/3''/5''}$), 6.86 (4 H, d, $J = 8.6$; $H^{2/6/2''/6''}$)	262
4,4‴-dimethoxy-1,1′:4′,1″:4″,1‴-quaterphenyl[b]	7.70 (12 H, m; $H^{3/5/3'''/5'''/2'/3'/5'/6'/2''/3''/5''/6''}$), 7.04 (4 H, d, $J = 8.8$; $H^{2/6/2'''/6'''}$), 3.81 (6 H, s; OMe)	366
4,4‴-dihydroxy-1,1′:4′,1″:4″,1‴-quaterphenyl[b]	9.62 (2 H, s; OH), 7.71 (8 H, m; $H^{2'/3'/5'/6'/2''/3''/5''/6''}$), 7.56 (4 H, d, $J = 7.8$; $H^{3/5/3'''/5'''}$), 6.88 (4 H, d, $J = 7.8$; $H^{2/6/2'''/6'''}$)	338

[a] Recorded in $CDCl_3$. [b] Recorded in DMSO-d_6. [c] Recorded in CD_2Cl_2. [d] Recorded in CD_3OD: the hydroxyl protons are not seen due to H/D exchange with the solvent.

Table 2. Characterization Data for **1**−**6**

	color	yield, %	anal.,[a] % C	H	N	FAB-MS data:[a] *m*/*z* for M^+	IR data, cm^{-1} ν_{B-H}	$\nu_{Mo=O}$	d_{Mo-Mo}, Å[b]
1	green	15	42.6 (43.2)	4.9 (4.8)	16.9 (16.9)	997 (998)	2547	949	9.08 (8.74)
2	green	20	47.1 (47.0)	4.8 (4.9)	15.6 (15.7)	1074 (1074)	2543	951	12.98
3	green	20	50.1 (50.1)	5.3 (4.9)	14.4 (14.6)	1150 (1150)	2546	950	16.57
4	green	20	52.5 (52.9)	5.1 (4.9)	13.3 (13.7)	1226 (1226)	2545	950	21.25
5	blue/purple	54	48.3 (48.0)	5.5 (5.1)	15.5 (15.3)	1103 (1104)	2544	947	12.98
6	purple/black	50	43.2 (43.4)	5.2 (4.9)	17.1 (16.9)	996 (998)	2548	949	7.59 (7.57)

[a] Calculated values in parentheses. [b] Calculated from a molecular mechanics energy-minimized structure. Values derived from crystal structures for **1** and **6** are in parentheses.

Table 3. Crystallographic Data for **1**·$2Et_2O$ and **6**·$3CH_2Cl_2$

	1·$2Et_2O$	**6**·$3CH_2Cl_2$
empirical formula	$C_{44}H_{68}B_2Cl_2Mo_2N_{12}O_6$	$C_{39}H_{54}B_2Cl_8Mo_2N_{12}O_4$
fw	1145.5	1252.0
space group	*Pnnm* (No. 58)	$P2_1/n$ (No. 14)
a, Å	24.566(11)	15.984(3)
b, Å	8.085(4)	16.934(3)
c, Å	14.172(4)	20.931(3)
β, deg	90	105.33(1)
V, Å^3	2815(2)	5464(2)
Z	2	4
ρ_{calc}, g cm^{-3}	1.352	1.522
μ, mm^{-1}	0.593	0.899
T, K	293(2)	173(2)
λ, Å	0.710 73	0.710 73
R_1, wR_2[a,b]	0.083, 0.220	0.048, 0.129

[a] Structure was refined on F_o^2 using all data; the value of R_1 is given for comparison with older refinements based on F_o with a typical threshold of $F \geq 4\sigma(F)$. [b] $wR_2 = [\sum[w(F_o^2 - F_c^2)^2]/\sum w(F_o^2)^2]^{1/2}$ where $w^{-1} = [\sigma^2(F_o^2) + (aP)^2 + bP]$ and $P = [\max(F_o^2,0) + 2F_c^2]/3$. For **1**·$2Et_2O$, $a = 0.074$, $b = 7.9693$; for **6**·$3CH_2Cl_2$, $a = 0.0525$, $b = 16.6281$.

(crystal size $0.5 \times 0.5 \times 0.3$ mm^3) 24 997 data were collected to $2\theta_{max} = 50°$ which after merging gave 9536 independent data ($R_{int} = 0.035$). Data were corrected for Lorentz and polarization effects and for absorption effects by an empirical method based on multiple measurements of equivalent data. Details of the crystal parameters and refinement are in Table 3. The structures were solved by conventional direct methods (SHELXTL) and were refined by the full-matrix least-squares method on all F^2 data (SHELX93) using Silicon Graphics Indigo R4000 and Indy computers.[10] All non-hydrogen atoms were refined anisotropically (with one exception; see below); hydrogen atoms were included in calculated positions and refined with isotropic thermal parameters. Atomic coordinates are given in Tables 4 and 6, and selected bond lengths and angles, in Tables 5 and 7.

Complex **1** is centrosymmetric, and the O and Cl atoms are disordered (50:50) between the two coordination sites. The atoms were refined separately, with a similarity restraint (SIMU) applied to the displacement parameters. The Cl atom was refined with anisotropic displacement parameters, but the O atom could only be refined isotropically. Attempts to apply restraints (DFIX) to the Mo−O and Mo−Cl bond lengths were unsuccessful, so these bond lengths were allowed to refine unrestrained; the resulting values are highly distorted by the disorder and should not be taken at face value. There is half a molecule of ether in each asymmetric unit which lies astride a mirror plane, with the oxygen atom in the plane. The carbon and oxygen atoms were refined anisotropically; the hydrogen atoms were included in calculated positions with their coordinates allowed to ride on those of the parent carbon atoms and were given fixed isotropic thermal parameters.

In **6**, where the two metals are crystallographically independent, the O and Cl atoms are ordered at one site but disordered (55:45) at the

Table 4. Atomic Coordinates ($\times 10^4$) and Equivalent Isotropic Displacement Parameters (Å^2 $\times$ 10^3) for the Complex Molecule of **1**·$2Et_2O$

	x	*y*	*z*	*U*(eq)
Mo(1)	1592(1)	7418(1)	0	71(1)
Cl(1)	1152(4)	8742(11)	1056(6)	91(2)
O(1)	1337(7)	8462(27)	1105(16)	67(6)
B(1)	2932(6)	6803(18)	0	60(4)
N(11)	2802(4)	8640(11)	0	53(2)
N(12)	2270(3)	9162(10)	0	54(2)
C(13)	2291(6)	10845(13)	0	68(3)
C(14)	2809(5)	11374(16)	0	73(4)
C(15)	3125(5)	9997(16)	0	64(3)
C(16)	1746(7)	11923(18)	0	110(6)
C(17)	3743(5)	9841(18)	0	84(4)
N(21)	2682(3)	5995(8)	876(4)	57(2)
N(22)	2126(3)	6032(7)	1012(5)	55(2)
C(23)	2036(4)	5176(11)	1812(6)	72(3)
C(24)	2521(5)	4649(13)	2195(7)	87(3)
C(25)	2915(4)	5143(11)	1599(7)	72(3)
C(26)	1458(4)	4961(14)	2183(8)	103(4)
C(27)	3525(4)	4882(14)	1635(8)	106(4)
O(30)	1112(3)	5541(9)	0	68(2)
C(31)	567(5)	5300(14)	0	61(3)
C(32)	357(5)	3769(17)	0	89(5)
C(33)	−194(4)	3455(14)	0	97(5)

(10) SHELXTL PLUS and SHELX93 program systems from Siemens Analytical X-Ray Instruments, Madison, WI.

Table 5. Selected Bond Lengths (Å) and Angles (deg) for **1**·2Et_2O

Mo(1)−O(30)	1.921(7)	Mo(1)−N(12)	2.183(8)
Mo(1)−O(1)	1.89(2)[a]	Mo(1)−N(22)	2.243(6)
Mo(1)−Cl(1)	2.134(8)[a]	Mo(1)−N(22′)	2.243(6)
O(1)−Mo(1)−Cl(1′)	100.9(5)	O(1)−Mo(1)−O(30)	98.6(7)
O(1)−Mo(1)−N(12)	88.0(6)	O(1)−Mo(1)−N(22)	83.5(6)
O(1)−Mo(1)−N(22′)	161.6(6)	Cl(1′)−Mo(1)−O(30)	94.9(3)
Cl(1′)−Mo(1)−N(12)	93.6(3)	Cl(1′)−Mo(1)−N(22)	174.3(2)
Cl(1′)−Mo(1)−N(22′)	95.6(3)	O(30)−Mo(1)−N(12)	168.1(3)
O(30)−Mo(1)−N(22)	88.0(2)	O(30)−Mo(1)−N(22′)	88.0(2)
N(12)−Mo(1)−N(22)	82.9(2)	N(12)−Mo(1)−N(22′)	82.9(2)
N(22)−Mo(1)−N(22′)	79.5(3)	Mo(1)−O(30)−C(31)	136.1(7)

[a] O/Cl disorder renders these distances highly inaccurate.

other. There are three molecules of CH_2Cl_2 in the asymmetric unit. One of these is disordered and was best modeled with the carbon atom fixed in one position with two alternative arrangements for the chlorine and hydrogen atoms. These disordered atoms were grouped and the site occupancies allowed to refine, with the total being fixed to 1. The resulting fractional site occupancies were 0.55 and 0.45, the same as the O/Cl disorder.

Results and Discussion

Ligand Syntheses. Of the bridging ligands we used, 1,3- and 1,4-dihydroxybenzene and 4,4′-dihydroxybiphenyl are commercially available. 2,2′-Dimethyl-4,4′-dihydroxybiphenyl, which is an analogue of 4,4′-dihydroxybiphenyl but with a larger dihedral twist imposed due to the steric effects of the methyl groups, was prepared by a homocoupling[8] of 3-methyl-4-bromoanisole followed by demethylation of the methoxy groups.[9] The more extended bridging ligands 4,4″-dihydroxyterphenyl and 4,4‴-dihydroxyquaterphenyl were prepared by reaction of 2 equiv of the Grignard reagent 4-$MeOC_6H_4MgBr$ with 1,4-dibromobenzene and 4,4′-dibromobiphenyl, respectively, using Ni(dppe)Cl_2 as a coupling catalyst, again followed by demethylation of the methoxy groups. These syntheses are summarized in Scheme 1. The ligand set allows evaluation of the effects on the metal−metal interactions of (i) increased metal−metal separation by means of additional aromatic spacers, (ii) increased dihedral twist between aromatic rings in the bridge, and (iii) the change in substitution pattern between 1,3- and 1,4-dihydroxybenzene.

Preparation and Characterization of Complexes. The complexes were readily prepared by reaction of 2 equiv of [Mo(O)(Tp*)Cl_2] with 1 equiv of the appropriate bridging ligand H_2L in toluene, with Et_3N present to deprotonate the phenols.[5] The yields of the reactions are variable (Table 2), and the reactions produce varying amounts of byproducts which presumably arise from traces of moisture in the reaction. In each case, the desired product [{Mo(O)(Tp*)Cl}$_2$(μ-L)] is the obvious major fraction and is the first to elute when the crude mixture is chromatographed (silica/CH_2Cl_2). Impurities which generally follow include the partially-oxidized Mo(V)/Mo(VI) complex [{Mo(O)(Tp*)Cl}(μ-L){$Mo(O)_2$(Tp*)}] (green) and the oxo-bridged dinuclear species [{Mo(O)(Tp*)Cl}$_2$(μ-O)], which is red; these oxidized species presumably arise from residual traces of moisture and/or oxygen in the solvent. Traces of mononuclear complexes [{Mo(O)(Tp*)Cl}(HL)], in which only one of the two phenol sites has a metal fragment attached, are the last to elute. These byproducts were all identified on the basis of their FAB mass spectra and IR spectra but not pursued further. The formulations of complexes **1**−**6** were confirmed by FAB mass spectra, IR spectra, and elemental analyses (Table 2). FAB mass spectrometry was a particularly suitable tool, since, in addition to molecular ions of the correct mass, the isotopic patterns of the peak clusters are quite characteristic and consistent with the expected formulations.

Table 6. Atomic Coordinates ($\times 10^4$) and Equivalent Isotropic Displacement Parameters (Å^2 $\times$ 10^3) for the Complex Molecule of **6**·3CH_2Cl_2

	x	*y*	*z*	*U*(eq)
Mo(1)	−539(1)	12516(1)	4073(1)	33(1)
Mo(2)	661(1)	9504(1)	1797(1)	30(1)
O(1)	−152(2)	11696(2)	3572(1)	36(1)
O(2A)	219(12)	12281(13)	4858(9)	44(4)
O(2B)	−1502(5)	12125(6)	4169(3)	36(2)
Cl(1A)	−1718(2)	11788(3)	4167(2)	41(1)
Cl(1B)	434(4)	12223(3)	5047(3)	38(1)
B(1)	−721(3)	14360(3)	3482(2)	30(1)
N(21)	−1360(2)	13809(2)	2993(2)	28(1)
N(22)	−1307(2)	13007(2)	3107(2)	30(1)
C(23)	−1856(3)	12662(2)	2582(2)	37(1)
C(24)	−2262(3)	13242(3)	2139(2)	41(1)
C(25)	−1931(3)	13958(2)	2413(2)	34(1)
C(26)	−2152(3)	14773(3)	2142(2)	46(1)
C(27)	−1958(3)	11783(3)	2516(3)	54(1)
N(31)	−923(2)	14319(2)	4167(2)	29(1)
N(32)	−917(2)	13603(2)	4480(2)	31(1)
C(33)	−1146(2)	13741(3)	5048(2)	33(1)
C(34)	−1288(3)	14542(3)	5095(2)	37(1)
C(35)	−1144(2)	14896(2)	4539(2)	33(1)
C(36)	−1212(3)	15747(3)	4348(2)	43(1)
C(37)	−1223(3)	13100(3)	5516(2)	43(1)
N(41)	202(2)	14056(2)	3549(2)	30(1)
N(42)	437(2)	13316(2)	3809(2)	32(1)
C(43)	1267(3)	13195(3)	3782(2)	37(1)
C(44)	1554(3)	13851(3)	3508(2)	40(1)
C(45)	868(3)	14382(2)	3358(2)	35(1)
C(46)	812(3)	15174(3)	3037(2)	45(1)
C(47)	1740(3)	12447(3)	4009(3)	52(1)
O(3)	282(2)	9260(2)	2579(1)	37(1)
O(4)	106(2)	10378(2)	1514(1)	43(1)
Cl(2)	1968(1)	10035(1)	2435(1)	46(1)
B(2)	626(3)	7987(3)	770(2)	33(1)
N(51)	−297(2)	8212(2)	814(2)	34(1)
N(52)	−399(2)	8790(2)	1246(2)	32(1)
C(53)	−1250(3)	8818(3)	1229(2)	39(1)
C(54)	−1686(3)	8249(3)	790(2)	48(1)
C(55)	−1074(3)	7869(3)	536(2)	43(1)
C(56)	−1182(4)	7214(3)	49(3)	60(1)
C(57)	−1612(3)	9381(3)	1636(3)	51(1)
N(61)	1055(2)	8724(2)	559(2)	32(1)
N(62)	1146(2)	9406(2)	923(2)	30(1)
C(63)	1477(3)	9955(3)	596(2)	37(1)
C(64)	1602(3)	9621(3)	24(2)	44(1)
C(65)	1334(3)	8856(3)	10(2)	38(1)
C(66)	1317(4)	8231(3)	−502(2)	56(1)
C(67)	1643(4)	10788(3)	831(3)	54(1)
N(71)	1147(2)	7726(2)	1461(2)	30(1)
N(72)	1289(2)	8260(2)	1979(2)	30(1)
C(73)	1709(3)	7866(2)	2526(2)	35(1)
C(74)	1838(3)	7086(3)	2357(2)	42(1)
C(75)	1474(3)	7014(2)	1693(2)	36(1)
C(76)	1401(3)	6300(3)	1261(3)	50(1)
C(77)	1978(4)	8231(3)	3197(2)	51(1)
C(11)	−130(3)	10896(2)	3601(2)	32(1)
C(12)	111(3)	10498(2)	3095(2)	32(1)
C(13)	106(3)	9674(2)	3084(2)	32(1)
C(14)	−123(3)	9247(3)	3579(2)	39(1)
C(15)	−357(4)	9652(3)	4077(2)	51(1)
C(16)	−362(3)	10471(3)	4099(2)	44(1)

The metal−metal separations were calculated for all of the complexes by molecular mechanics energy minimizations using MM2 parameters[11] and are included in Table 2. In addition, the computed structures suggest that in **2** the dihedral twist between the two aromatic rings of the bridging ligand is

(11) The calculations were performed on a CAChe workstation (CAChe Scientific, Beaverton, OR, 1994) using the programs supplied. Structures were energy-minimized using the molecular mechanics package with an extended MM2 parameter set. The ZINDO program (written by M. C. Zerner) was run using the INDO/1 parameters.

Scheme 1. Syntheses of the New Ligands

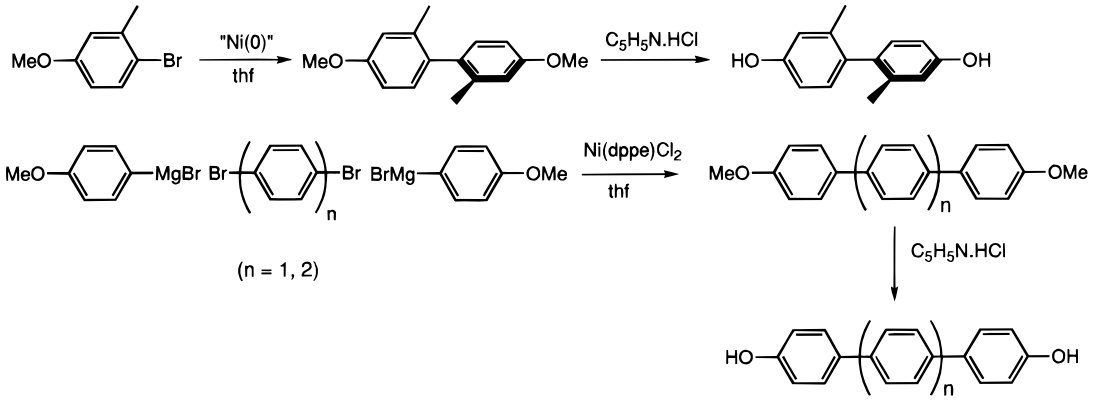

Table 7. Selected Bond Lengths (Å) and Angles (deg) for **6**·$3CH_2Cl_2$

Mo(1)−O(2A)	1.81(2)[a]	Mo(1)−O(2B)	1.735(10)[a]
Mo(1)−O(1)	1.938(3)	Mo(1)−N(32)	2.179(3)
Mo(1)−N(22)	2.229(3)	Mo(1)−N(42)	2.243(3)
Mo(1)−Cl(1A)	2.303(5)[a]	Mo(1)−Cl(1B)	2.269(5)[a]
Mo(2)−O(4)	1.747(3)	Mo(2)−O(3)	1.934(3)
Mo(2)−N(52)	2.151(3)	Mo(2)−N(62)	2.173(3)
Mo(2)−N(72)	2.321(3)	Mo(2)−Cl(2)	2.3410(12)
O(2A)−Mo(1)−O(1)	95.8(7)	O(4)−Mo(2)−O(3)	102.90(12)
O(2A)−Mo(1)−N(22)	168.9(7)	O(4)−Mo(2)−N(62)	92.36(13)
O(2A)−Mo(1)−N(42)	90.8(7)	O(4)−Mo(2)−N(72)	169.59(13)
N(22)−Mo(1)−N(42)	78.66(12)	N(62)−Mo(2)−N(72)	80.46(11)
N(32)−Mo(1)−Cl(1A)	95.84(13)	N(52)−Mo(2)−Cl(2)	168.25(9)
O(2A)−Mo(1)−N(32)	91.1(7)	O(4)−Mo(2)−N(52)	92.12(14)
O(1)−Mo(1)−N(22)	87.37(12)	O(3)−Mo(2)−N(62)	163.18(12)
O(1)−Mo(1)−N(42)	87.49(12)	O(3)−Mo(2)−N(72)	83.45(11)
O(2A)−Mo(1)−Cl(1A)	99.9(7)	O(4)−Mo(2)−Cl(2)	99.47(11)
N(22)−Mo(1)−Cl(1A)	90.59(12)	N(62)−Mo(2)−Cl(2)	92.67(9)
O(1)−Mo(1)−N(32)	167.88(12)	O(3)−Mo(2)−N(52)	87.43(12)
N(32)−Mo(1)−N(22)	84.06(12)	N(52)−Mo(2)−N(62)	84.94(12)
N(32)−Mo(1)−N(42)	82.45(12)	N(52)−Mo(2)−N(72)	79.81(12)
O(1)−Mo(1)−Cl(1A)	92.79(13)	O(3)−Mo(2)−Cl(2)	91.78(10)
N(42)−Mo(1)−Cl(1A)	169.23(12)	N(72)−Mo(2)−Cl(2)	88.45(9)
C(11)−O(1)−Mo(1)	134.4(2)	C(13)−O(3)−Mo(2)	136.4(2)

[a] O/Cl disorder renders these distances highly inaccurate.

37°—which is typical for a biphenyl-type fragment[12]—whereas in **5** the steric interaction between the methyl substituents forces the rings to be nearly perpendicular (87° dihedral angle). These values correspond to the lowest computed energies of the complexes but in fluid solution at room temperature will of course vary over a wide range. However they do suggest that the extent of coupling between the π systems of the two aromatic rings in the bridge will be significantly less for **5** than for **2**.

Crystal Structures. Complexes **1** and **6** afforded X-ray-quality crystals when recrystallized from CH_2Cl_2/ether mixtures, and the structures of the complex units of **1**·$(Et_2O)_2$ and **6**·$(CH_2Cl_2)_3$ are shown in Figures 2 and 3, respectively (see also Tables 4−7). In **1**·$(Et_2O)_2$ the dinuclear complex is centrosymmetric. A particular problem with this structure is the presence of disorder involving the Cl and O atoms. The electron density map showed the presence of two peaks of equivalent intensity and at a distance from the Mo atom intermediate between the distances expected for Mo^V−Cl and Mo^V═O bonds (*ca.* 2.4 and 1.7 Å, respectively).[6] Refinement of the site occupancies for the Cl and O atoms at these positions converged at values close to 0.5 and 0.5, so the site occupancies were then fixed at these values. The resulting Mo═O and Mo−Cl bond lengths are, as a result, very inaccurate: the apparent Mo−Cl distance

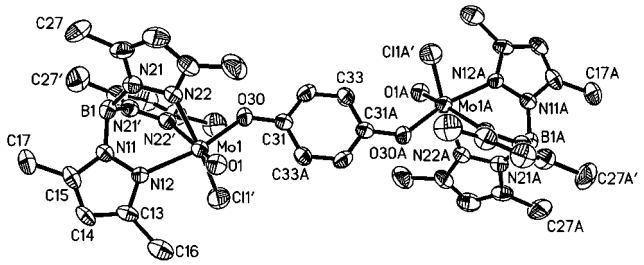

Figure 2. Crystal structure of the metal complex in **1**·$(Et_2O)_2$ (the O/Cl disorder is not shown).

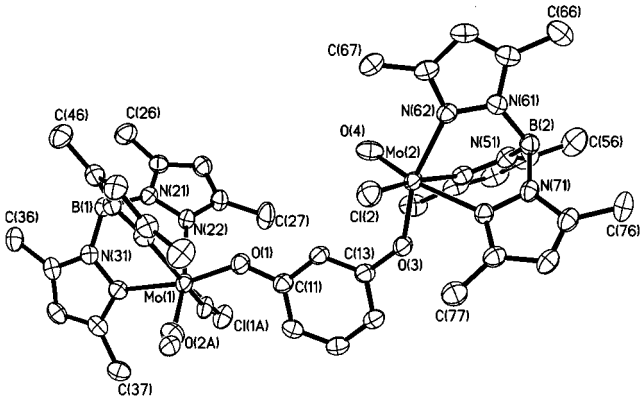

Figure 3. Crystal structure of the metal complex in **6**·$(CH_2Cl_2)_3$, showing the resolved components of the O/Cl disorder at Mo(1).

(2.13 Å) is too short, and the apparent Mo═O distance (1.89 Å) is too long. The other structural parameters however are as accurate as could be expected from such a small crystal. There is also a crystallographic plane of symmetry through the molecule, which includes the bridging ligand, the Mo atoms, and the pyrazolyl rings containing atoms N(11)/N(12) and N(11A)/N(12A). The labelling scheme used in Figure 2 denotes atoms related by the inversion center with a suffix A, such as N(22) and N(22A), and atoms related by the mirror plane with a ′ (prime), such as N(22) and N(22′). The metal−metal distance is 8.74 Å.

Since there are two possible arrangements for the Cl and O atoms at each metal center, there are in principle four possible arrangements in total, but the requirement for a center of symmetry reduces this to two, of which only one is shown in Figure 2. A disorder of this type arises because the metal centers are chiral, and a dinuclear complex therefore consists of a mixture of two diastereoisomers. If they crystallize together, as they have done here, then a 50:50 mixture of the two components inevitably gives rise to the observed disorder. The encapsulating nature of the Tp* ligand partially shields the O and Cl atoms from intramolecular interactions which make the

(12) (a) Eaton, V. J.; Steele, D. *J. Chem. Soc., Faraday Trans. 2* **1973**, 1601. (b) Brock, C. P.; Minton, R. P. *J. Am. Chem. Soc.* **1989**, *111*, 4586.

Table 8. Electrochemical and Electronic Spectral Data for **1**−**6**

complex	electrochemical processes[a,b]		electronic spectral data:[a] λ_{max}/nm ($10^{-3}\epsilon$/M^{-1} cm^{-1})			
	oxidations	reductions				
1	+1.25,[c] +0.26	−1.19, −1.44		658 (5.1)	397 (8.1)	266 (17.7)
2	+0.92, +0.44	−1.13[d]		616 (6.7)	389 (14.5)	272 (33.1)
3	+0.74, +0.56	−1.16[d]		592 (5.4)	373 (15.9)	297 (30.6)
4	+0.61[d]	−1.16[d]		587 (5.1)	380 (sh)[f]	311 (33.0)
5	+0.78, +0.55	−1.21[d]		571 (5.9)	364 (14.6)	262 (28.0)
6	+0.58[e]	−1.20, −1.40		544 (3.3)	360 (sh)[f]	266 (19.4)
Mo(Tp*)(O)Cl(OPh)[g]	+0.68	−1.21	760 (0.1)	520 (1.8)	350 (5.8)	

[a] All measurements made in CH_2Cl_2. [b] The electrochemical measurements were made at a Pt-bead working electrode containing 0.1 M $^nBu_4NPF_6$ as base electrolyte, using a scan rate of 0.2 V s^{-1}. All potentials are quoted vs the ferrocene/ferrocenium couple which was used as an internal standard. All processes are chemically reversible one-electron transfers with peak−peak separations in the range 80−120 mV unless stated otherwise. [c] This process occurred at the limit of the solvent window in a region of high background current, so its reversibility could not be established; the peak potential was taken from a square-wave voltammogram. [d] Two coincident, chemically reversible, one-electron processes. [e] Totally irreversible process (no return wave). [f] sh = shoulder. [g] Measured under the same conditions for comparison purposes.

disorder more likely; we have noted a similar disorder on other Mo(Tp*) complexes.[4d] It is noteworthy that it was this type of disorder, between Mo═O and Mo−Cl groups, that led to the recent controversy over the possible existence of "bond-stretch isomers".[13]

In the structure of complex **6**, the two metal centers are crystallographically independent. Again, the two diasteroisomers have cocrystallized, but in this case the resulting O/Cl disorder need only be expressed at one metal center because the requirement for a centrosymmetric arrangement is removed. Because of the better quality of the crystal, the disorder could be resolved rather better than in **1**. The two Mo═O bond lengths at the disordered site were found to be 1.735(10) and 1.81(2) Å, with the two Mo−Cl bond lengths being 2.269(5) and 2.303(5) Å. These may be compared with the (more trustworthy) values of 1.747(3) and 2.341(1) Å, respectively, for the Mo═O and Mo−Cl distances at the ordered site [Mo(2)]. The metal−metal distance is 7.57 Å.

Electrochemical and Molecular Orbital Properties. The mononuclear complex [Mo(O)(Tp*)Cl(OPh)] was reported by Enemark *et al.* to undergo a chemically reversible one-electron reduction in MeCN at −0.59 V vs Ag/AgCl.[5] The reduction is metal centered and is therefore a Mo(V)/Mo(IV) couple. We reinvestigated this complex, as it is a mononuclear analogue of our dinuclear complexes **1**−**6**. We observed the expected reduction, at −1.21 V vs the ferrocene/ferrocenium couple (Fc/Fc^+) in CH_2Cl_2, but we also observed a chemically reversible (equal cathodic and anodic peak currents; peak−peak separation 90 mV) one-electron *oxidation* at +0.68 V vs Fc/Fc^+ which was not reported before (Table 8). It seems reasonable to assign this to a metal-centered Mo(V)/Mo(VI) couple; this is supported by the molecular orbital analysis of the complexes (*vide infra*).

The dinuclear complexes would therefore be expected to have two oxidations, corresponding to stepwise oxidation of the Mo(VI)/Mo(VI) species, and two reductions, corresponding to stepwise reduction to the Mo(IV)/Mo(IV) species. The electrochemical data, summarized in Table 8, confirm this. Representative voltammograms are shown in Figure 4. For **1**, the two oxidations are separated by 990 mV and the two reductions are separated by 250 mV. That the first oxidation is a one-electron process was confirmed coulometrically, and since the other three waves in the voltammograms are of the same intensity, these too are confirmed as one-electron processes: in any event this is the only chemically sensible assigment. The interaction between the centers being oxidized is therefore extremely strong, with K_c for the mixed-valence Mo(V)/Mo(VI) state being *ca.* 10^{17}, one of the largest electrochemical interactions recorded.[1] The interaction between the centers when they are reduced is less spectacular but still significant, with $K_c = 2 \times 10^5$ for the mixed-valence Mo(IV)/Mo(V) species (K_c is the comproportionation constant for the mixed-valence state, i.e. the equilibrium constant for the reaction given in eq 1). If the oxidations and reductions were both wholly metal-localized, then we would expect the interaction between the two oxidations and the interaction between the two reductions to be comparable on simple electrostatic grounds. Our results suggest that the oxidations are partly delocalized onto the bridging ligands, whereas the reductions are more metal-localized. This is not unreasonable since the dianion of 1,4-dihydroxybenzene may be oxidized to *p*-benzoquinone, so the resonance structures [Mo(VI)−(dihydroxybenzene dianion)−Mo(VI)] and [Mo(V)−(*p*-benzoquinone)−Mo(V)] could both be contributions to the fully oxidized species. Partial delocalization of the additional positive charges onto the bridging ligand would bring them closer together and thereby increase the interaction between them; in contrast, the bridging ligand cannot easily be further reduced, so the electrons added by reduction reside in metal-localized orbitals.

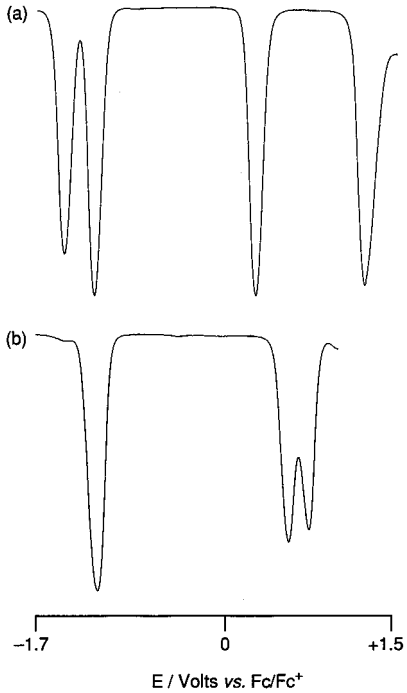

Figure 4. Square-wave voltammograms of (a) **1** and (b) **3** in CH_2Cl_2.

$$[Mo^{V}Mo^{V}] + [Mo^{VI}Mo^{VI}] \rightarrow 2[Mo^{V}Mo^{VI}] \qquad (1)$$

(13) Yoon, K.; Parkin, G.; Rheingold, A. *J. Am. Chem. Soc.* **1991**, *113*, 1437.

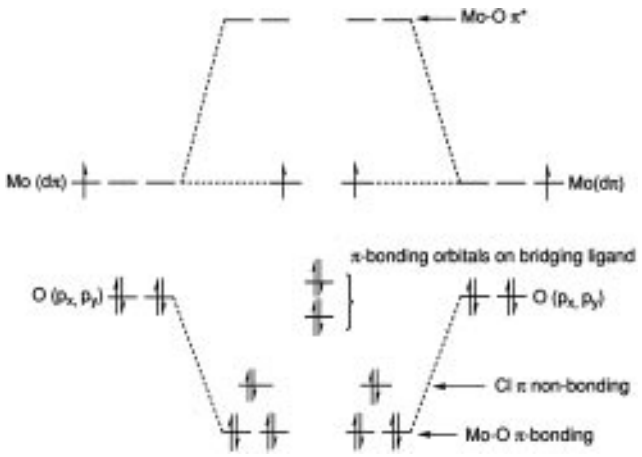

Figure 5. Frontier molecular orbital diagram of **1**.

A qualitative MO picture of the frontier orbitals of **1** is shown in Figure 5. This is based on a combination of the known spectroscopic properties of oxomolybdenum(V) complexes[14,15] and our observed electrochemical and EPR results (*vide infra*) and is also in agreement with a ZINDO computation.[11] Of the three d(π) orbitals of the Mo atoms, two interact strongly with the π-donor p orbitals of the oxo ligand to give Mo═O π-bonding (filled) and π-antibonding (empty) levels; the HOMOs [singly occupied, since Mo(V) is d^1] are the remaining—largely unperturbed—d(π) nonbonding orbitals of each Mo atom, and these are essentially degenerate (the molecular orbitals will be the sum and difference combinations of these two d orbitals). The other two d orbitals (σ*) of each metal will lie above the Mo═O (π*) levels and are not shown. If the Mo═O axis is taken as the local *z* axis, then the configuration of the metal centers is d_{xy}^1.

The important feature of the MO picture that makes **1** significantly different from simple oxomolybdenum(V) complexes is the presence of π-bonding orbitals of the bridging ligand; the HOMO of the bridge lies close to, but below, the singly-occupied metal d_{xy} levels. Given the inaccuracy in determining absolute energies, it was not clear from the ZINDO calculation alone whether this orbital lay above or below the two metal d orbitals. However, that they must lie below the molybdenum d(π) levels is quite clear from the EPR spectra and electronic spectra of the complexes (see later) which confirm that the unpaired electrons are metal-localized. If the bridging ligand HOMO were above the two molybdenum d(π) orbitals, then the complex would be a diamagnetic Mo(IV)—(quinone)—Mo(IV) species, which clearly it is not. Oxidation of the metals is therefore not very different in energy from oxidation of the bridging ligand, and the oxidized Mo(VI)—(p-$OC_6H_4^{2-}$)—Mo(VI) species has some Mo(V)—(quinone)—Mo(V) character mixed with it. In contrast, the only alternative reduced structure which could mix with the Mo(IV)/Mo(IV) species arises from occupation of the Mo═O π* levels, which are sufficiently high in energy for such a contribution to be slight and which in any case do not involve delocalization across the bridging ligand. The π* levels of the bridging ligand are far too high in energy to contribute to the structure of the reduced complex; the reductions are therefore metal-localized.

As the number of aromatic spacers in the bridge increases (from complex **1** to complex **4**), the electrochemical interactions decrease rapidly. The separations between the two oxidation waves for **1**—**3** are 990, 480, and 180 mV, respectively, and finally for **4** the two oxidations cannot be resolved and have merged to give a single wave. For the reductions, the two processes are unresolvable for **2**—**4**. The general behavior that the separation between the oxidation processes is much greater than the separation between the reduction processes is maintained. It is interesting that this is the reverse of the behavior observed for electrochemical interactions between {Mo(NO)(Tp*)Cl} fragments in dinuclear complexes, when it is the reductions (partially delocalized onto the bridging ligands) that are split and the metal-localized oxidations that are coincident.[4a,4e]

Comparison of **5** with **2** shows the effect of using bulky ligand substitutents to impose a dihedral twist between the two aromatic rings of the bridge: the separation between the two oxidations has decreased from 480 mV in **2** (37° dihedral twist) to 230 mV in **5** (87° dihedral twist). This confirms that the oxidations involve to some degree the bridging ligand π orbitals, since if the oxidations were solely metal-based the resulting through-space interaction would not change significantly between **2** and **5**. A comparable result was obtained when 3,3′-dimethyl-4,4′-bipyridine was used instead of 4,4′-bipyridine as a bridge between two {Mo(NO)(Tp*)Cl} fragments: the additional imposed dihedral twist approximately halved the electrochemical interaction.[4e] Comparison of **1** with **6** shows the effect of changing the substitution pattern of the bridge (from 1,4 to 1,3). The interaction between the two reductions is slightly reduced, from 250 to 200 mV, which is in keeping with a variety of other dinuclear complexes where it has been shown that a 1,3-substituted bridge is less effective than a 1,4-substituted bridge at transmitting electronic interactions.[16] Also, two reversible oxidations no longer occur: there is just one totally irreversible oxidation. This is consistent with the partial ligand-centered character of the oxidations, since among these dinuclear complexes the bridging ligand of **6** is unique in not being able to form a quinone-type structure by oxidation.

Electronic Spectra. Electronic spectral data are summarized in Table 8. Simple oxomolybdenum(V) complexes such as $[Mo(O)Cl_5]^{2-}$ can in principle display three d—d transitions in which the single unpaired electron is promoted from the d_{xy} orbital to the (doubly-degenerate) Mo═O(π*) level or the two higher d(σ*) levels.[14,15] The lower two of these occur at approximately 710 and 435 nm; the highest is obscured by the lowest-energy charge-transfer band. The charge-transfer bands were originally thought to arise from promotion of electrons from the filled Mo═O(π) levels to the d orbitals,[14] but on the basis of more recent work these charge-transfer transitions are now considered to be Cl(π) → Mo(d_{xy}).[15] In our dinuclear complexes however there are two types of transition which complicate this simple picture. The first is the possibility of phenolate-to-Mo ligand-to-metal charge-transfer (lmct) which, on the basis of Figure 5, should be the lowest-energy charge-transfer band; the second is $\pi \rightarrow \pi^*$ transitions within the bridging ligands and within the pyrazolyl rings of the Tp* ligand.

The intense lowest energy transition in **1**—**6** at 540—660 nm has no counterpart in the spectrum of $[Mo(O)Cl_5]^{2-}$, and we ascribe this to a phenolate—to—Mo(V) lmct band, on the basis both of the intensity of the peaks and the MO picture described above for complex **1**. As the number of aromatic rings in the bridge increases between complexes **1** and **4**, this band is steadily blue-shifted, indicating a steady lowering of the energy of the bridging ligand π orbital as the conjugated network

(14) Gray, H. B.; Hare, C. R. *Inorg. Chem.* **1962**, *1*, 363.
(15) (a) So, H.; Pope, M. T. *Inorg. Chem.* **1972**, *11*, 1441. (b) Carducci, M. D.; Brown, C.; Solomon, E. I.; Enemark, J. H. *J. Am. Chem. Soc.* **1994**, *116*, 11856. (c) Sabel, D. M.; Gewirth, A. A. *Inorg. Chem.* **1994**, *33*, 148.
(16) (a) Wlodarczyk, A.; Maher, J. P.; McCleverty, J. A.; Ward, M. D. *J. Chem. Soc., Chem. Commun.* **1995**, 2397. (b) Richardson, D. E.; Taube, H. *J. Am. Chem. Soc.* **1983**, *105*, 40.

becomes more extended. In complexes **5** and **6**, where the dihedral twist (for **5**) or the *meta* substitution pattern (for **6**) makes the bridging ligands more like electronically isolated monophenols, this lmct band moves to higher energy (*cf.* the position of the lmct band for mononuclear [Mo(O)(Tp*)(OPh)-Cl], Table 8).[5] The transitions at 350−400 nm are at positions consistent with their being the lowest-energy Cl(π) → Mo(d_{xy}) lmct band (*cf.* ≈370 nm for $[Mo(O)Cl_5]^{2-}$).[14,16] Finally, the highest-energy bands appear likely to be $\pi \rightarrow \pi^*$ transitions in the bridging ligands. These transitions decrease steadily in energy from **1** to **4** as the more extended conjugated network results in a decrease of the HOMO/LUMO gap of the bridging ligand: the variation in the energies of the $\pi \rightarrow \pi^*$ transitions matches that of the phenolate-to-Mo(V) lmct bands across the series of complexes.

For mononuclear [Mo(O)(Tp*)(OPh)Cl] a weak peak at 760 nm was ascribed to the expected metal-centered d−d transition[5] [strictly, it is a transition from the d_{xy} orbital to the Mo═O(π^*) levels]. Similar transitions would also be expected for **1**−**6** at similar energies, but they are evidently masked by the intense phenolate-to-Mo(V) lmct bands, which are both more intense for the dinuclear complexes than for [Mo(O)(Tp*)(OPh)Cl] and are also at lower energy and therefore nearer the expected position of the lowest d−d band. The observation that for [Mo-(O)(Tp*)(OPh)Cl] the phenolate-to-Mo(V) lmct band is somewhat higher in energy than the d−d band is in agreement with the MO picture in Figure 5, in which the energy of the highest ligand-based π orbital is slightly below that of the metal-centered HOMO.

EPR Spectroscopic Properties. The isotropic solution EPR spectrum of the mononuclear model complex [Mo(O)(Tp*)Cl-(OPh)] gives the typical "singlet plus sextet" pattern characteristic of mononuclear Mo complexes (the sextet arises from the *ca.* 25% of Mo nuclei that have $I = {}^5/_2$).[4,5] We found g_{iso} to be 1.939(1) and the hyperfine coupling A_{Mo} in the sextet to be 50.4 G (45.7×10^{-4} cm^{-1}), both in good agreement with Enemark's results.[5] The behavior of the dinuclear complexes **1**−**6** is quite different from that of the mononuclear complex, consistent with the presence of magnetic exchange interactions between the unpaired spins. Three features of the spectra confirm the presence of magnetic exchange interactions: (i) the more complex hyperfine coupling pattern, (ii) the presence of line broadening, and (iii) the presence of $\Delta m_s = 2$ transitions at the half-field position (g ≈ 3.9). Representative spectra at room temperature and at 77 K are shown in Figures 6 and 7, respectively, and the relevant spectral parameters are summarized in Table 9.

Complexes **4** and **3**, which have the largest metal−metal separations, give essentially identical solution spectra which contain all the components to be expected for coupling of the unpaired electrons to both nuclei, *i.e.* a singlet (from the $I = 0$, $I = 0$ isotopomers), a 1:1:1:1:1:1 sextet (from the $I = 0$, $I =$ 5/2 isotopomers), and a 1:2:3:4:5:6:5:4:3:2:1 undecet (from the $I = 5/2$, $I = 5/2$ isotopomers). Only the outermost components of the undecet are clearly resolved, but their relative intensities and positions are as expected (Figure 6, top). In addition, the separation between signals in the multiplets has halved to 25.1 G (22.7×10^{-4} cm^{-1}), which is exactly the behavior expected when both electrons are coupled equally to both Mo nuclei.[4] The positions of the signals are the same as in the mononuclear model complex. The frozen-solution spectra (at 77 K) were broad and relatively featureless. Although complexes **4** and **3** have two unpaired electrons, no $\Delta m_s = 2$ transition was observed at the half-field position for either complex, either at room temperature or at 77 K, which we ascribe to the large

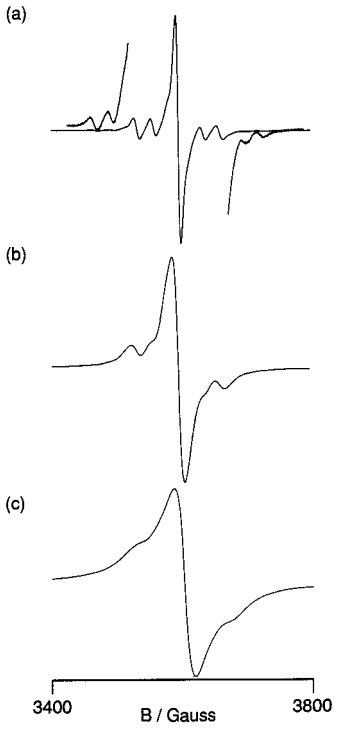

Figure 6. Solution EPR spectra of (a) **4**, (b) **2**, and (c) **6** in CH_2Cl_2, showing the steadily increasing broadening.

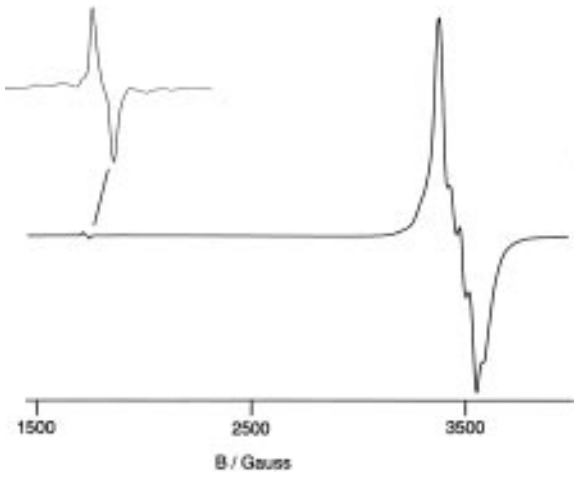

Figure 7. Frozen-solution (77 K) EPR spectrum of **6** in a CH_2Cl_2/thf glass, showing the $\Delta m_s = 2$ transition.

metal−metal separation. In summary, the spectra of these complexes are exactly like those of the many magnetically-coupled dinuclear molybdenum complexes based on {Mo(NO)-(Tp*)(Cl)} fragments which we examined recently.[4]

For complex **2** the room-temperature spectrum is noticeably broadened (Figure 6, middle). The central singlet and the sextet are still apparent, but the broadening has made them less distinct: the peak−peak separation for the central singlet is now 21 G, compared to *ca.* 9 G for both **3** and **4**. The weak outlying components of the undecet, which were clear for **3** and **4**, are broadened to the extent that they are invisible. The main transition of the frozen-solution spectrum is again rather broad and featureless, but a weak $\Delta m_s = 2$ transition is now apparent at g = 3.89 whose relative intensity compared to the $\Delta m_s = 1$ transition is *ca.* 5×10^{-5}. For complex **5**, which has the same metal−metal separation as **2** but a larger twist in the bridging ligand, the room-temperature spectrum reverts to the "normal" behavior of **3** and **4**: the additional broadening that was apparent in the spectrum of **2** has disappeared (the peak−peak separation

Table 9. Summary of the EPR Spectral Properties for **1**−**6**

complex	g_{iso}[a]	peak width, G[a]	A_{Mo}, $cm^{-1} \times 10^4$ (G)	$g(\Delta m_s = 2)$[b]	intensity of $\Delta m_s = 2$[b,c]
1	1.94	≈300	not resolved	3.90	5×10^{-4}
2	1.939	21	22.8 (25.2)	3.89	5×10^{-5}
3	1.939	9.5	22.8 (25.1)		
4	1.939	8.8	23.0 (25.4)		
5	1.938	9.7	23.8 (26.3)	3.88	5×10^{-5}
6	1.939	35	not resolved	3.89	5×10^{-4}

[a] Taken from room-temperature solution spectra. [b] Taken from 77 K frozen-glass spectra. [c] Ratio of the intensities of the $\Delta m_s = 2$ and $\Delta m_s = 1$ signals.

for the central singlet is 9.7 G), and the outer components of the hyperfine undecet are again clearly resolved. We can conclude that the interaction responsible for the spectral broadening seen for **2** is transmitted in part through the π system of the bridging ligand. The weak $\Delta m_s = 2$ transition is however still apparent in the 77 K spectrum of **5** and has an intensity comparable to that of **2**; the intensity of this is therefore dependent only on metal−metal separation, and is independent of the conformation of the bridging ligand.

In complex **1**, not only is the metal−metal separation even shorter, but the bridging ligand is necessarily planar. The solution EPR spectrum of **1** is barely detectable and consists just of a single very weak, very broad signal with a peak−peak separation of *ca.* 300 G. No hyperfine coupling is resolved. The 77 K spectrum is similarly broad and featureless, but there is a $\Delta m_s = 2$ transition at $g = 3.91$ whose intensity is *ca.* 5×10^{-4} times that of the main transition and is therefore (very approximately) 10 times more intense than those of **2** and **5** relative to the main transition. Finally, for complex **6** a more well-defined room-temperature spectrum occurs. The peak−peak separation is 35 G, which is more than for **2**−**5** but substantially less than for **1**. Shoulders arising from hyperfine coupling to the molybdenum nuclei are just apparent (Figure 6, bottom). Considering the small metal−metal separation in **6**, the presence of a $\Delta m_s = 2$ transition is expected, and indeed such a transition is observed with an intensity comparable to that of **1**. However the resolution of this transition in the spectrum of **6** is much better than that of **1** and an expansion of the $\Delta m_s = 2$ transition of **6** (Figure 7) shows the presence of hyperfine coupling which that of **1** does not.

Thus, we see two trends in the series of EPR spectra. First, a $\Delta m_s = 2$ transition at 77 K becomes apparent and grows in intensity as the metal centers approach each other. The presence of this transition is not related to the extent of communication through the π system of the bridge, as it does not significantly change in intensity between **2** and **5** or between **1** and **6**. Second, the extent of broadening of the room-temperature spectra also becomes more significant as the bridging ligands shorten. However the extent of this is related to the properties of the π system of the bridging ligand (again, compare **2** with **5** and **1** with **6**) and not just metal−metal separation.

When interpreting the EPR spectra of dinuclear paramagnetic complexes, one needs to consider the effects of both the dipolar and anisotropic interactions,[17] both of which contribute to the zero-field splitting. The dipolar interaction D_{dip} is responsible for the appearance of the $\Delta m_s = 2$ transitions. In the "point charge" approximation—assuming that the unpaired electrons are fully metal-localized, which is reasonable here—the magnitude of the dipolar interaction is given by eq 2, where r is the

$$D_{dip} = g^2(\mu_B)^2/r^3 \qquad (2)$$

electron−electron (*i.e.* metal−metal) separation. According to this approximation, D_{dip} therefore varies only with the metal−metal separation and is not dependent on the properties of any bridging group other than its length. This accounts for the relative intensities of the $\Delta m_s = 2$ transitions for **2** and **5** and for **1** and **6**. The large error associated with measuring the intensities of the very weak $\Delta m_s = 2$ transitions unfortunately precludes any quantitative attempt to relate their intensities to the metal−metal separations.

A note of caution needs to be sounded at this point. In practice, the magnitude of the dipolar interaction can depend also on the relative orientations of the local axes of the two interacting metal centers,[18] since the unpaired electrons are in orbitals which are not spherically symmetric (this corresponds to a breakdown of the point-charge approximation). Thus for **2** and **5** the different average dihedral twists of the aromatic bridging ligands could result in different relative orientations between the local z axes, i.e. the O═Mo···Mo═O dihedral angle will be different in each case, which could be responsible for the fact that the spectrum of **2** is broader than that of **5** despite having the same metal−metal separation. However in fluid solution there is also the possibility of free rotation about the Mo−O and/or O−C bonds of the phenolate linkage, which would remove this problem. A molecular mechanics study of the model mononuclear complex [Mo(Tp*)(O)Cl(OPh)] showed that the barrier to rotation of the phenyl group about the C−O bond is only *ca.* 20 kJ mol^{-1}, which is sufficiently low to consider that there is effectively free rotation about this bond at room temperature in fluid solution. We believe therefore that the difference in the EPR signal width between **2** and **5** in fluid solution is unlikely to arise from noncoincidence of the local axes, as they will be averaged.

Broadening of the signal arises from the presence of zero-field splitting, since the $m_s = -1 \rightarrow m_s = 0$ and $m_s = 0 \rightarrow m_s = 1$ transitions will become slightly different in energy, leading to two closely-spaced lines rather than one (fine structure), each with its own hyperfine pattern. If these are not resolved, the result will be homogeneous line broadening. Since both the dipolar and anisotropic interactions contribute to zero-field splitting, either (or both) of them could in principle be responsible for the broadening we observe in the EPR spectra of **1**−**6**. However the dependence of signal width on the nature of the π pathway linking the metals means that it cannot be due to the dipolar interaction.

The anisotropic interaction takes account of the mixing of electronic ground and excited states *via* spin−orbit coupling. In a d^1−d^1 dinuclear complex with a d_{xy}/d_{xy} ground state, the lowest excited state arises from promotion of one electron to a d_{xz} or d_{yz} orbital [really a π^* orbital involving a Mo d(π) orbital and a p orbital of the oxo ligand; Figure 5]. The π orbitals of the aromatic spacer must therefore play a crucial role in the anisotropic exchange interaction, since the energy of the excited state will depend on the extent of π delocalization between the

(17) Bencini, A.; Gatteschi, D. *EPR of Exchange Coupled Systems;* Springer-Verlag: Berlin, 1990.

(18) Chow, C. D.; Willett, R. D. *J. Chem. Phys.* **1973**, *59*, 5903.

metal centers, and this fact accounts for the observed relation between the signal width and the properties of the bridging ligand. Delocalization across the bridge will be decreased by (i) increasing the length of the bridge (complexes **1**−**4**), (ii) imposition of a substantial dihedral twist between two aromatic rings within the bridge (compare **2** and **5**), and (iii) changing the substitution pattern from *para* to *meta* (compare **1** and **6**).[16] The changes in signal width exactly mirror these characteristics of the bridging ligands.

Clearly it will be desirable to have quantitative magnetic data (values of *J*) for the dinuclear complexes, so that the magnitudes of the exchange interactions can be related to the properties of the bridging ligands, as we have done for dinuclear {Mo(NO)(Tp*)Cl} complexes with bis(pyridyl) bridging ligands.[4f] We are currently pursuing this, along with a more detailed EPR study at various different field strengths, and the results will be reported in a future paper.

Conclusion

We have prepared a series of dinuclear complexes in which redox-active, paramagnetic $\{Mo^{V}(O)(Tp^*)Cl\}^{+}$ fragments are attached to either end of one of a series of diphenol bridging ligands. There are strong electrochemical interactions which result in substantial splittings between the successive Mo(V)/Mo(VI) oxidations, and smaller splittings between the successive Mo(V)/Mo(IV) reductions. The difference in the splittings between the two oxidations and the reductions is due to the fact that the oxidations are partly delocalized onto the bridging ligand, such that the resonance form Mo(V)−(quinone)−Mo(V) contributes to the oxidized species, whereas the reductions are essentially metal-localized. EPR spectra show that magnetic exchange effects are present, resulting in both line broadening in the room-temperature (solution) spectra arising from the anisotropic interaction between the electrons and the appearance of half-field ($\Delta m_s = 2$) transitions in the 77 K (frozen) spectra arising from the dipolar interaction between the electrons. The electrochemical interactions decrease as the bridging ligands become longer; similarly, changing the substitution pattern of the bridge from *para* to *meta* or imposing a substantial dihedral twist between phenyl rings of the bridging ligand decreases the electrochemical interactions. The anisotropic interaction responsible for the line broadening in the EPR spectra is dependent on the nature of the π pathway between the metal centers in the same way.

Acknowledgment. We thank the EPSRC for a studentship (V.Â.U.) and for equipment grants to purchase the EPR spectrometer and the diffractometer. Mr. Tim Branston is also thanked for assistance with synthesizing some of the bridging ligands. The reviewers of an earlier version of this paper are acknowledged for some helpful comments.

Supporting Information Available: Tables of X-ray experimental details and crystallographic data, all atomic coordinates, anisotropic thermal parameters, and bond distances and angles for **1**·$2Et_2O$ and **6**·$3CH_2Cl_2$ (17 pages). Ordering information is given on any current masthead page.

IC951634N